Improving photovoltaic efficiency of $Cu_2BaSn(S, Se)_4$/CdS solar cells using SCAPS

D. Kumar

Department of Physics, School of Chemical Engineering and Physical Sciences,

Lovely Professional University, Phagwara, Punjab, India.

ABSTRACT

$Cu_2BaSn(S, Se)_4$ (CBTSSe) absorber based thin film solar cells (TFSC) have been analyzed using 1D-SCAPS (Solar cell capacitance simulator) program. In this article, the efficiency of the TFSC is improved by optimizing the acceptor density and electron affinity of CBTSSe. The optimized device demonstrates power conversion efficiency (η) = 16.4%, open circuit voltage (V_{OC}) = 928 mV, short circuit current density (J_{SC}) = 24 mA/cm^2 and fill factor (FF) = 74.5 %.

INTRODUCTION

$Cu_2BaSn(S, Se)_4$ (CBTSSe) a quaternary compound has drawn notable attention for CBTSSe TFSC because of its optimum band gap, high absorption coefficient, p-type conductivity etc. The compound can be considered as a potential replacement of $Cu_2ZnSn(S, Se)_4$ TFSC. The maximum photovoltaic (PV) efficiency of CZTSSe achieved is 12.6% [1] which is limited due to the high V_{OC}-deficit which is associated with the Cu-Zn cation disordering. The disordering is caused due to the similar crystal radius of Cu^+ (0.74 Å) and Zn^{2+} (0.74 Å) respectively for IV-fold coordination in CZTS crystal. Defect analysis of CZTSSe reveals that Cu substitution on Zn site (Cu_{Zn}) exhibits lower formation energy than copper vacancy (V_{Cu}) as the small size mismatch between Cu^+ and Zn^{2+} ions and the similar structural (tetrahedral) environment for Cu and Zn. As Zn^{2+} and Sn^{4+} (0.69 Å) also have nearly same size and consequently, it creates deep level Zn_{Sn} or Sn_{Zn} antisite defects [2]. Presence of the defects results in a large number of localized states in band gap and also non-radiative recombination centers/traps. Therefore, Cu_{Zn} and Zn_{Sn} antisite disordering is the major challenge for the large V_{OC} deficit – a key performance-limited factor. CZTSSe solar cells show V_{OC} deficit more than 600 mV [3] whereas CIGS cells shows V_{OC} deficit of 500 mV [4]. Several approaches have been attempted to solve disordering issue in kesterite based CZTSSe such as; doping with Cu-substituents: $(Cu,Ag)_2ZnSn(S,Se)_4$, doping with Zn-substituents or replacement of Zn: $Cu_2(Cd,Zn)Sn(S,Se)_4$, Cu_2MnSnS_4, Cu_2FeSnS_4, Cu_2CoSnS_4, etc. The Ag-doping is limited due to the variation of n-type and p-type conductivity of the semiconductor and also availability of Ag on the earth crust is very low (0.08 ppm). On the other hand, Zn-doping or replacement is less favorable due to toxic nature, low abundance (0.15 ppm) of Cd, and multiple valence states for manganese, iron and cobalt which create deep level in the band gap. $(Cu,Ag)_2ZnSn(S,Se)_4$ and $Cu_2(Cd, Zn)Sn(S,Se)_4$ absorber based solar cells have achieved maximum PV efficiency 11.2% [5] and 11.5% [6] respectively.

A classic approach has been adopted to overcome the issues of cation disordering and band tailing by introducing different coordination environments into the parent structure moving away from a tetrahedral coordination environment (as in the case of zinc-blende derived structures: CZTS, cations are tetrahedrally coordinated). This approach involves replacement of Zn atoms by divalent alkaline-earth (AE) elements forming the Cu_2-AE-Sn-Ch_4 chalcogenides (AE = Ba/Sr and Ch = S/Se) with trigonal (for Ch = S; space group $P3_1$) or orthorhombic (for Ch = Se; space group *Ama2*) structure [7]. The size of AE elements Sr (1.4 Å) and Ba^{2+} (1.56 Å) is larger than that of the Cu^{+} (0.74 Å) and Sn^{4+} (0.69 Å). Moreover, the coordination environment of the Cu_2-AE-Sn-Ch_4 chalcogenides is different from the CZTS (tetrahedral coordination for all cation) which can suppress the band tailing. Shin *et al* further demonstrate by PL and external quantum efficiency (EQE) measurements that the band tailing in CBTSSe is low[8]. The FWHM of the PL peak centered at 805 nm for $Cu_2BaSnSSe_3$ is ≈60 nm much smaller than the FWHM for CIGSSe (≈100 nm) and CZTSSe (≈190 nm). Moreover, the shift between the PL peak (1.54 eV) and the band gap (1.55 eV) evaluated from the EQE measurement is about 10 meV which is smaller compared to the shifts determined for CIGSSe (30 meV) and CZTSSe (100 meV). This implies a low degree of band tailing in CBTSSe compounds possibly due to the different crystal size of cations and coordination environments which inhibit the formation of Cu_{Ba} and Sn_{Ba} antisite disordering.

In the present work, the current density-voltage (JV) is analyzed using one dimension solar cell capacitance simulator (1D-SCAPS) program.

MODELLING OF TFSC

The numerical simulation is carried out on Mo/CBTSSe(p-type)/CdS(n-type)/ZnO/AZO (in substrate configuration) using 1D-SCAPS [9]. The parameters used for optimization the device are given in Table 1.

Table 1 Parameters of CBTSSe, CdS, ZnO and ITO used for the optimization of the device.

	CBTSSe	**CdS**	**ZnO**	**ITO**
Thickness (μm)	2.5	0.05	0.05	0.2
Electron affinity (eV)	Varied	4.2	4.55	4.7
Band gap (eV)	1.4	2.45	3.3	3.4
Dielectric permittivity (relative)	9	8.9	8.12	8.12
N_C (cm^{-3})	1.75×10^{18}	1.00×10^{18}	1.00×10^{18}	1.00×10^{18}
N_V (cm^{-3})	3.41×10^{19}	$1.00E\times10^{18}$	1.00×10^{18}	1.00×10^{18}
μ_e ($cm^2/V/s$)	100	50	100	100
μ_h ($cm^2/V/s$)	10	20	20	20
N_A (cm^{-3})	Varied	----------	----------	----------
N_D (cm^{-3})	----------	1×10^{17}	1×10^{10}	1×10^{20}
A (cm^{-1} $eV^{1/2}$)	1×10^{4}	5×10^{4}	5×10^{4}	1×10^{5}

$V_{th,\,n}$ (cm/s)	10^7	10^7	10^7	10^7
$V_{th,\,h}$ (cm/s)	10^7	10^7	10^7	10^7
	CBTSSe	**CdS**	**ZnO**	**ITO**

Device structure: Mo/CBTSSe/CdS/ZnO/ITO.

Working point conditions

Temperature 300.00 K

AM1.5 G Illumination

Surface work function of Mo (back contact): 5.5 eV

Electron SRV: 10^7 cm/s

Hole SRV: 10^5 cm/s

RESULT AND DISCUSSION

In the optimization of device, acceptor density (hole density) and electron affinity of CBTSSe is varied. The acceptor density is varied from 10^{13} cm^{-3} to 10^{19} cm^{-3}. It is observed in Fig. 1 (a) that V_{OC} of the device increases with the increase of carrier density and then decreases when the acceptor density exceeds 10^{17} cm^{-3}. As acceptor density increases, quasi-Fermi level (acceptor energy level) shifts towards the valence band maxima, consequently the difference between quasi Fermi levels increases. The large difference in the quasi Fermi levels corresponds to the large V_{OC}. After a critical acceptor density, CBTSSe transforms to the degenerate state wherein the recombination lifetimes and thus diffusion length of minority carriers decreases. Another effect of heavily doping is to increase tunneling current due to the reduction in the junction width. The increase of tunneling current results in decrease of $V_{OC.}$

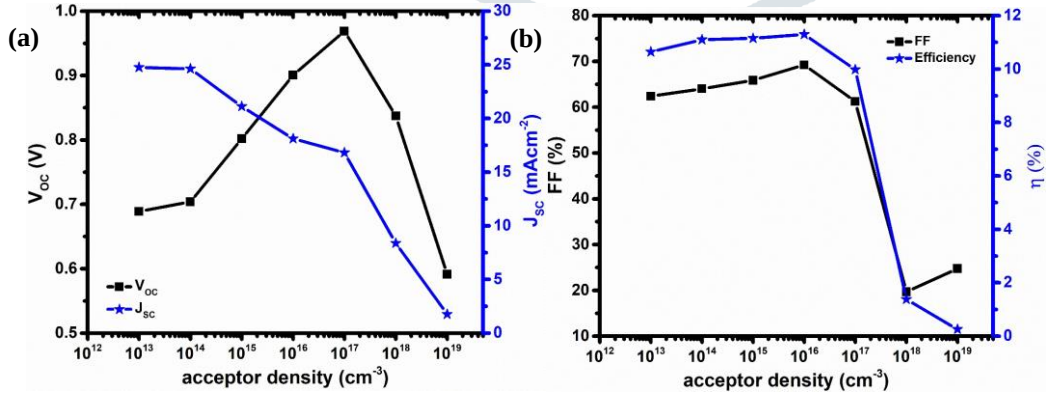

Fig. 1 (a) Variation of V_{OC} and J_{SC} (b) FF and η with acceptor density of CBTSSe absorber layer.

The effect of acceptor density on the short circuit current density (J_{SC}) is different from the behavior of V_{OC}. J_{SC} decreases with the increase of (Fig. 1 (a)) acceptor density which is due to the increase of recombination rate (SRH

recombination). The similar behavior in fill factor (FF) and PV efficiency (η) is seen in Fig. 1 (b). The maximum PV efficiency is obtained 11.3% at acceptor density 10^{16} cm^{-3}.

The second optimization is carried out by varying electron affinity (4 eV to 4.6 eV) of the absorber layer (CBTSSe) to investigate band alignment at CBTSSe/CdS interface shown in Fig. 2. The electron affinity of a material depends on deposition conditions and post-deposited treatments.

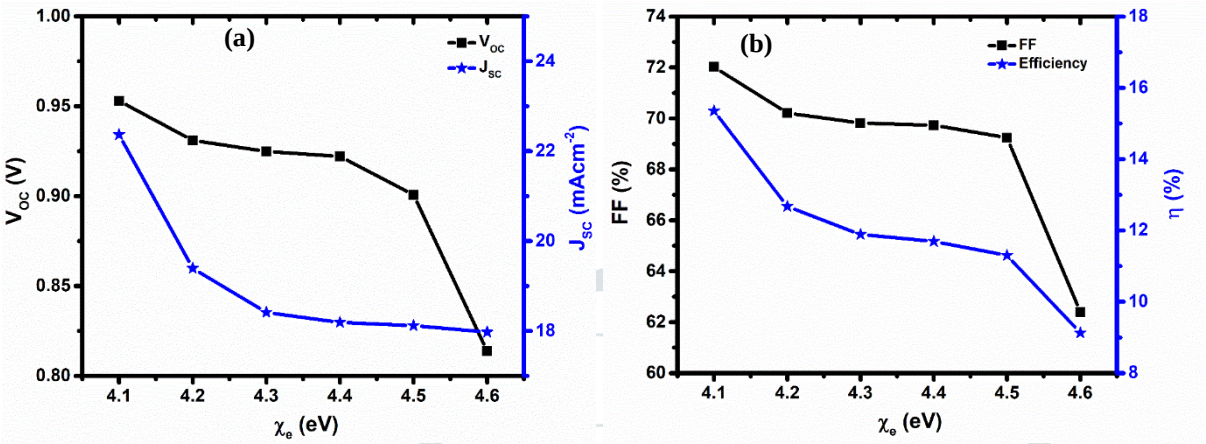

Fig. 2 (a) Variation of V_{OC} and J_{SC} (b) FF and η with electron affinity of CBTSSe absorber layer.

It indicates the decrease of J_{SC}, V_{OC}, FF and η with the increase of electron affinity of CBTSSe. This behavior is anticipated due to the increase in the conduction band offset ($CBO = \chi_{CBTSSe} - \chi_{CdS}$ where χ is electron affinity) increases from -0.1 to 0.4 eV. The negative CBO corresponds to the cliff-like offset and positive CBO corresponds to the spike-like offset at the CBTSSe/CdS interface. With the increase of χ the spike is increased which acts as a barrier and inhibits flow of the photo-generated minority carriers. The cliff-like offset is responsible for the recombination of the minority carriers at the interface. The maximum efficiency obtained is 15.4% at CBO = -0.1 eV.

Table 2 Parameter of layers of optimized TFSC.

	CBTSSe	**CdS**	**ZnO**	**ITO**
Thickness (μm)	2.5	0.05	0.05	0.2
Electron affinity (eV)	4.1	4.2	4.55	4.7
Band gap (eV)	1.4	2.45	3.3	3.4
Dielectric permittivity (relative)	9	8.9	8.12	8.12
N_C (cm^{-3})	1.75×10^{18}	1.00×10^{18}	1.00×10^{18}	1.00×10^{18}
N_V (cm^{-3})	3.41×10^{19}	$1.00E\times10^{18}$	1.00×10^{18}	1.00×10^{18}
μ_e (cm^2/V/s)	100	50	100	100

μ_h (cm^2/V/s)	10	20	20	20
N_A (cm^{-3})	1.00×10^{16}	----------	----------	----------
N_D (cm^{-3})	----------	1×10^{17}	1×10^{10}	1×10^{20}
A (cm^{-1} $eV^{1/2}$)	1×10^{4}	5×10^{4}	5×10^{4}	1×10^{5}
$V_{th,\,n}$ (cm/s)	10^7	10^7	10^7	10^7
$V_{th,\,h}$ (cm/s)	10^7	10^7	10^7	10^7
	CBTSSe	**CdS**	**ZnO**	**ITO**

After optimization of acceptor density and electron affinity of CBTSSe, JV characteristics of the optimized cell are analyzed. The parameters used to analyze the JV characteristics are given in Table 2.

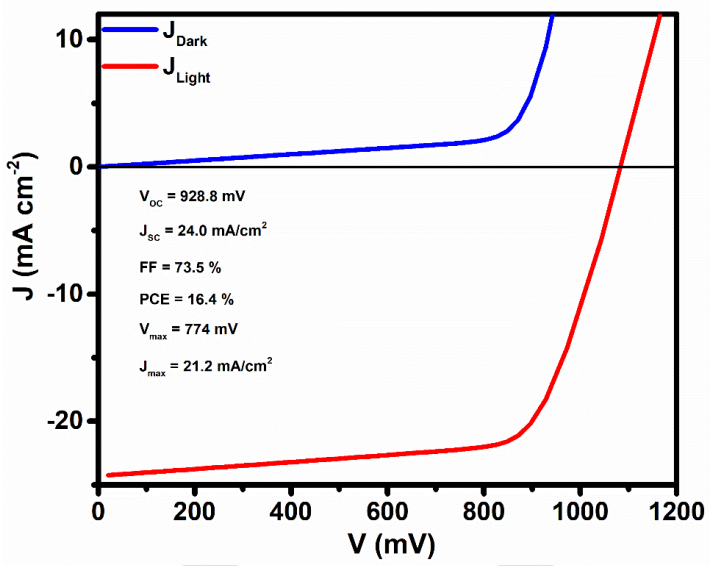

Fig. 3 JV characteristics of the CBTSSe solar cell with optimized device parameters.

The maximum efficiency of the optimized cell achieved is 16.4 % with V_{OC} = 928 mV, J_{SC} = 24 mA/cm^2 and FF = 73.5 % as obtained from Fig. 3. The large V_{OC} demonstrates that the V_{OC}-deficit is 472 mV which significantly lesser than the reported elsewhere [2], [3]. It is important to note that there is no JV crossover from JV-light region to the JV-dark. The band representation of the optimized device is presented in Fig. 4. The device shows the cliff behavior at the interface of CBTSSe/CdS.

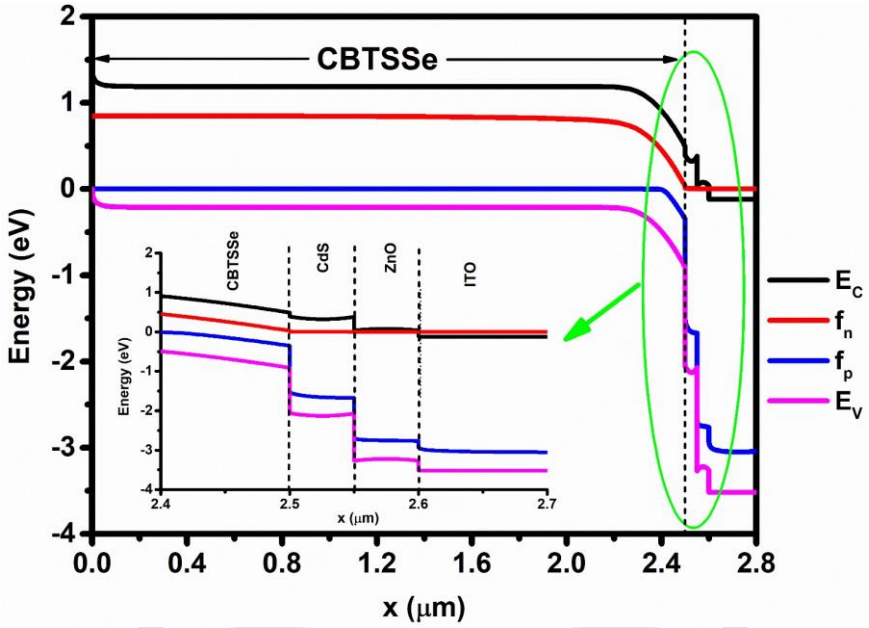

Fig. 4 Band diagram of the CBTSSe solar cell with optimized device parameters.

CONCLUSION

The CBTSSe absorber based solar cell (Mo/CBTSSe/CdS/ZnO/ITO) is analyzed using 1D-SCAPS program. First, CBTSSe solar cell is simulated by varying acceptor density and electron affinity of CBTSSe separately. These parameters influence the device characteristics strongly. Later, the optimized acceptor density (10^{16} cm^{-3}) and electron affinity (4.1 eV) is used to simulate the device. The maximum photovoltaic efficiency achieved is 16.4 % with V_{OC} = 928 mV, J_{SC} = 24 mA/cm^2 and FF = 73.5 % with a low open circuit voltage deficit. The device shows the cliff behavior at the interface of CBTSSe/CdS.

REFERENCES

[1] W. Wang *et al.*, "Device characteristics of CZTSSe thin-film solar cells with 12.6% efficiency," *Adv. Energy Mater.*, vol. 4, no. 7, pp. 1–5, 2014.

[2] F. Hong, W. Lin, W. Meng, and Y. Yan, "Trigonal Cu_2-II-Sn-VI_4 (II = Ba, Sr and VI = S, Se) quaternary compounds for earth-abundant photovoltaics," *Phys. Chem. Chem. Phys.*, vol. 18, no. 6, pp. 4828–4834, 2016.

[3] T. K. Todorov *et al.*, "Beyond 11% efficiency: Characteristics of state-of-the-art $Cu_2ZnSn(S,Se)_4$ Solar Cells," *Adv. Energy Mater.*, vol. 3, no. 1, pp. 34–38, 2013.

[4] S. Niki *et al.*, "CIGS absorbers and processes," *Prog. Photovoltaics Res. Appl.*, vol. 18, no. 6, pp. 453–466, 2010.

[5] Y. Qi *et al.*, "Elemental Precursor Solution Processed $(Cu_{1-x}Ag_x)_2ZnSn(S,Se)_4$ Photovoltaic Devices with

over 10% Efficiency," *ACS Appl. Mater. Interfaces*, vol. 9, no. 25, pp. 21243–21250, 2017.

[6] C. Yan *et al.*, "Beyond 11% Efficient Sulfide Kesterite $Cu_2Zn_xCd_{1-x}SnS_4$ Solar Cell: Effects of Cadmium Alloying," *ACS Energy Lett.*, vol. 2, no. 4, pp. 930–936, 2017.

[7] D. Shin, B. Saparov, T. Zhu, W. P. Huhn, V. Blum, and D. B. Mitzi, "$BaCu_2Sn(S,Se)_4$: Earth-abundant chalcogenides for thin-film photovoltaics," *Chem. Mater.*, vol. 28, no. 13, pp. 4771–4780, 2016.

[8] D. Shin, T. Zhu, X. Huang, O. Gunawan, V. Blum, and D. B. Mitzi, "Earth-Abundant Chalcogenide Photovoltaic Devices with over 5% Efficiency Based on a $Cu_2BaSn(S,Se)_4$ Absorber," *Adv. Mater.*, vol. 29, no. 24, pp. 1–7, 2017.

[9] M. Burgelman, P. Nollet, and S. Degrave, "Modelling polycrystalline semiconductor solar cells," *Thin Solid Films*, vol. 361, pp. 527–532, 2000.